Upset dynamics of an airliner model: a nonlinear bifurcation analysis

Stephen J. Gill, Mark H. Lowenberg and Simon A. Neild
Faculty of Engineering, University of Bristol, Bristol, BS8 1TR, UK

Bernd Krauskopf
Department of Mathematics, University of Auckland,
Private Bag 92019, Auckland 1142, New Zealand

Guilhem Puyou
Airbus France, 31060 Toulouse Cedex 03, France

Etienne Coetzee
Airbus Operations, Airbus, Bristol, BS99 7AR, UK

November 2012

Abstract

Despite the significant improvement in safety linked to the fourth generation of airliners, the risk of encountering upset conditions remains an important consideration. Upset — which may arise from faults, external events or inappropriate pilot inputs — can induce a loss-of-control incident if the pilot does not respond in the correct manner. Any initiative aimed at preventing such events requires an understanding of the fundamental aircraft behaviour. This paper presents the use of bifurcation analysis, complemented by time-history simulations, to understand the flight dynamics of the open loop NASA Generic Transport Model by identifying the attractors of the dynamical system that govern upset behaviour. A number of drivers for potential upset conditions have been identified, including non-oscillatory spirals and oscillatory spins. The analysis shows that these spirals and spins are connected in two-parameter space and that, by an inappropriate pilot reaction to the spiral, it is possible to enter the oscillatory spin.

Nomenclature

α	=	angle of attack
β	=	angle of sideslip
V	=	total velocity
p	=	roll rate
q	=	pitch rate
r	=	yaw rate
lat	=	latitudinal displacement
lon	=	longitudinal displacement
alt	=	vertical displacement
ϕ	=	roll angle
θ	=	pitch angle
ψ	=	yaw angle
u	=	x body axis velocity
v	=	y body axis velocity
w	=	z body axis velocity
δ_a	=	aileron deflection
δ_e	=	elevator deflection
δ_r	=	rudder deflection
δ_t	=	throttle setting
f	=	generic nonlinear function
$\mathbf{x}$	=	state vector
$\boldsymbol{\lambda}$	=	vector of parameters
c.g.	=	centre of gravity

1 Introduction

The introduction of the fourth generation of airliners has brought a significant improvement in flight safety [1]. However, the risk of encountering upset conditions remains an important consideration. Upset may arise in non-protected aircraft and, potentially, in flight envelope protected aircraft if protection is lost due to faults, external events or inappropriate pilot inputs. This can induce a loss of control event, currently the leading cause of civil aviation fatalities [2], if the pilot's actions are not effective to recover the upset condition. The activity receiving most attention in attempting to reduce upset events is improved pilot training; other initiatives include fully protected aircraft, prediction of upset to improve pilot awareness, and automation (from assisted to fully automated) to allow for easier recovery. Whichever solution is being studied, it is important to understand the fundamental aircraft behaviour in these highly nonlinear flight regimes.

In addition to the underlying nonlinear dynamics, upset and upset recovery are also linked to control law characteristics, including envelope protection functions. Today on Airbus aircraft, for example, in the nominal situation ('normal laws') the flight envelope is protected so that abnormal attitudes cannot be reached as a consequence of recorded atmospheric disturbances. However, for very low probability cases combining system fault events (that lead to a decrease in control law performance) and unusual external perturbations, or in the case of an extraordinary unpredictable external event (e.g. impact damage), the flight parameters may go beyond the limits of the protected envelope. In this case, specific control laws are activated to ensure aircraft recovery. These abnormal attitude control laws essentially consist of direct control on the pitch, roll and yaw axis with very basic and robust stability augmentation in the yaw case. The pilot can then apply classical upset recovery procedures; see for example Ref. [3].

A major objective of the next generation of fly-by-wire aircraft is to further increase safety whilst also improving handling qualities. One potential improvement is to provide the pilot with a higher level of automation even in extreme events, either by introducing advanced manual control laws or by fully automating the recovering procedures (as is already done for some military aircraft). To do so, models and methods for validation and

clearance of those new functions are required.

Upset prevention and recovery training is an important tool for reducing loss of control events and will become compulsory for US carriers in 2013 [4]. The industry-developed *Upset Recovery Training Aid* [3] is the most well known document outlining a training programme on upset recovery through piloted simulations. The programme gives pilots knowledge of upset conditions and of basic recovery procedures, practised on in-flight simulators, although this document has not yet been widely implemented. The International Committee for Aviation Training in Extended Envelopes (ICATEE) [5] and the Simulation of Upset Recovery in Aviation (SUPRA) [6] programmes also focus their upset prevention and recovery work on piloted simulations. However, the majority of flight simulators lack the necessary expanded aerodynamic envelope data. Currently, recovery procedure training would require extrapolation of the aerodynamic data from the operating envelope and this may result in significant errors and even the mis-modelling of key features of the dynamic response.

Effective upset training would need to fully identify all possible upset scenarios, which would not necessarily be shown by the use of simulators alone. Hence, analytical methods are required to complement the techniques developed for flight simulation. The NASA Aviation Safety Program was created to explore systems associated with the Next Generation Air Transportation System in order to help assure safety. Included in this programme was the development of the Generic Transport Model (GTM) in order to look at real in-flight upset dynamics and control without the risk attributed to the use of a full scale aircraft; the GTM is a 5.5% dynamically scaled aircraft [7]. Extensive wind tunnel tests were performed on the GTM airframe [8] to create an expanded-envelope aerodynamic data set for use in development of a Matlab Simulink model. It allows the development of control laws that can be implemented in real time on the GTM in-flight model. The majority of GTM research has been on the development of controllers [9, 10] to help prevent upset scenarios and for implementing into the Aircraft Integrated Resilient Safety Assurance and Failsafe Enhancement (AIRSAFE) concept, where resilient control is integrated with flight safety assessment and management; an overview is given in Ref. [11]. However, this control-based research is not based on a direct physical link to the causes of upset and the underlying flight dynamics of the GTM. Hence, these controllers may not work for all possible upset scenarios for the GTM.

It is the purpose of this paper to provide an overall understanding of the nonlinear flight mechanics that occurs under high angle of attack conditions. To that end, a bifurcation analysis of the GTM, complemented by time-history simulations, is presented. Full bifurcation analysis of civil airliner flight dynamics models is not common practice, although the same approach has been successfully applied to military aircraft [12, 13, 14]; moreover, it has been shown to be advantageous when compared to time simulation techniques for aircraft ground dynamics [15], landing gear shimmy [16] and landing gear mechanisms [17]. Bifurcation analysis has already been applied to the GTM in [18, 19]; however, these studies focused on control at specific bifurcation points rather than building up a comprehensive understanding of the flight dynamics of the GTM. Jung [20] implemented bifurcation analysis methods on the VELA1 blended wing body airliner model and, while it did facilitate a greater understanding of the aircraft's flight dynamics, it was principally concerned with using control allocation methods to improve handling. While some spin equilibrium solutions were identified, the aerodynamic data was limited to angles of attack of less than 25°. Bifurcation analysis was implemented on the extended envelope version of the SUPRA model [21]. Variation of the flight dynamics in multi-parameter space was investigated; however, as only equilibrium solutions were computed, the existence of other upset attractors, for example periodic orbits, was not addressed.

Murch [22, 23] identified post-stall and spin dynamic modes of the GTM. These spin tests were aimed primarily at discovery of the most accurate forced-oscillation and rotary balance blending function for use in the GTM Simulink model. For this, pro-spin rudder inputs of up to $\delta_r = \pm 30°$ were used, while other control parameters were zero or at the maximum physical deflection. Therefore, Refs. [22, 23] did not address why the GTM departs into spins and how the characteristics of the spins change as parameters are varied.

Bifurcation analysis is an appropriate method to determine insight into the overall behaviour of the model as it finds and then tracks different types of solutions throughout a parameter range; moreover, the different bifurcations can then be tracked in multi-dimensional parameter space. In this paper, as part of recent initiatives to apply this technique to the open-loop GTM behaviour [24, 25, 26], we present the application of bifurcation analysis to an eighth-order version of the NASA GTM to build an understanding of the underlying flight mechanics. The work identifies possible upset scenarios and, moreover, provides a deeper insight into the complex interactions that govern upset. This can then be focused on problems such as upset prediction and

design of prevention/recovery strategies.

2 Bifurcation and Continuation Analysis

Bifurcation and continuation analysis methods are based on the principles of dynamical systems theory; see, for example, Ref. [27, 28] as entry points to the literature. Solutions are found, and then tracked or *continued* numerically throughout a chosen parameter range in order to generate bifurcation diagrams, which highlight qualitative changes in the system's dynamic response.

2.1 Bifurcation theory

Bifurcation analysis is applied here to an autonomous dynamical system of the general form

$$\dot{\mathbf{x}} = f(\mathbf{x}, \boldsymbol{\lambda}), \tag{1}$$

where f is a set of n nonlinear differentiable functions, $\mathbf{x} \in \Re^n$ is the state vector and $\boldsymbol{\lambda} \in \Re^m$ is a vector of m parameters.

In aircraft open-loop flight dynamics, f would typically consist of the eighth-order rigid-body equations of motion ($\mathbf{x} = [\alpha, \beta, V, p, q, r, \phi, \theta]$); $\boldsymbol{\lambda}$ may include the control surface inputs (aileron, elevator, rudder, thrust) and/or other parameters, such as centre of gravity location. In numerical bifurcation analysis loci of steady-state solutions are mapped out over a specified range of values of one or more of the parameters, such as elevator deflection; these parameters are referred to as the *continuation parameter(s)*. A one-parameter bifurcation diagram of equilibria (stationary solutions) is generated by setting $\dot{\mathbf{x}} = f(\mathbf{x}, \boldsymbol{\lambda}) = \mathbf{0}$ and solving the resulting system of equations. Similar continuation (or path-following) methods can be used for finding branches of periodic solutions. Selected state components, $x_i, i = 1, ..., n$ are then plotted with respect to the continuation parameter. From these diagrams and using bifurcation theory, bifurcations of the system dynamics can be located and characterised. Various types of bifurcations may arise as parameter values vary, details of which are given in textbooks such as Ref. [27].

A bifurcation is defined as a qualitative change in the system dynamics as a parameter is varied. Mathematically, a bifurcation of an equilibrium occurs when an eigenvalue crosses the imaginary axis. Similarly, when one of its Floquet multiplier crosses the unit circle there is a bifurcation of a periodic orbit. In the results presented here, five types of bifurcations are discussed; they are all of codimension one, meaning that they are encountered when a single continuation parameter is varied. They are:

- A saddle node or limit point or fold bifurcation of equilibria occurs when a real eigenvalue crosses the imaginary axis. On one side of the bifurcation point (locally) there are no equilibria and on the other side there are two (for example, one stable and the other unstable).
- A Hopf bifurcation occurs when a complex pair of eigenvalues crosses the imaginary axis. Here, the equilibrium changes stability and a periodic orbit is created, which may be either stable or unstable.
- A limit point or fold bifurcation of periodic orbits, which arise when a real Floquet multiplier crosses the unit circle at $+1$; as for equilibria, on one side of the bifurcation (locally) there are no periodic orbits and on the other there are two.
- A period-doubling bifurcation occurs when a real Floquet multiplier crosses the unit circle at -1. The periodic orbit loses stability while a new periodic orbit with (approximately) twice the period is born.
- A Neimark-Sacker or torus bifurcation is where a periodic orbit loses stability when a pair of complex Floquet multipliers crosses the unit circle and an additional frequency of oscillation is introduced. The result is dynamics on a torus, which may be either periodic (locked) or quasi-periodic.

Continuation methods are the numerical implementation of bifurcation analysis [28]. These methods use a predictor-corrector technique in order to continue a steady-state solution (equilibrium or periodic orbit) as a parameter changes, to form paths of solutions over the parameter space; at each solution point local stability

Table 1: Notation as used in the figures.

———	Stable equilibrium	○	Hopf bifurcation
– – –	Unstable equilibrium	●	Torus bifurcation
———	Stable periodic orbit	■	Period doubling bifurcation
– – –	Unstable periodic orbit		

is computed from eigenvalues for equilibria and Floquet multipliers for periodic orbits. Bifurcations can be detected and also followed as parameters vary. The numerical nature of continuation methods requires that the model is smooth in $\mathbf{x}$ and $\boldsymbol{\lambda}$.

2.2 Continuation software AUTO and the Dynamical Systems Toolbox

A number of continuation software packages are available; this study uses AUTO [29], which is coded in FORTRAN. The package AUTO has been developed in the academic context, where it is widely used. The original version was developed in the 1980's with the latest version, AUTO07P, released in 2007. It has been applied to various aircraft dynamic problems, such as the analysis of ground dynamics [15], landing gear shimmy [16], landing gear mechanisms [17] and, in addition, to flight dynamics [30] and control [31].

AUTO has the capability, when applied to autonomous dynamical systems, to trace out stationary solutions from an initial starting point to map out the equilibria of the system ($\dot{\mathbf{x}} = f(\mathbf{x}, \boldsymbol{\lambda}) = \mathbf{0}$). While doing this, it is able to detect and label bifurcation points. AUTO also allows the continuation of periodic solutions from Hopf bifurcations or a known starting solution, which allows for the analysis of periodic oscillations. AUTO detects saddle node bifurcations of equilibria, Hopf, saddle node bifurcations of periodic orbits, torus and period-doubling bifurcations, and it can trace the loci of such bifurcation points in two parameters to create a *two-parameter bifurcation diagram*.

In this study, the version of AUTO incorporated into the Matlab Dynamical Systems Toolbox, developed by Coetzee *et al.* [32], was used. This version of AUTO runs the FORTRAN code from the Matlab environment. It uses object orientated coding to set up the problem and then connects to AUTO07P through .mex files. Although computationally more expensive than AUTO07P alone, the use of the Dynamical Systems Toolbox facilitates the setting up of the system in a Matlab or Simulink formulation with access to the associated functions and tools.

In the bifurcation diagrams presented here, we use AUTO to depict the stable/unstable equilibria, stable/unstable periodic orbits and bifurcations using the notation given in Table 1.

3 The NASA Generic Transport Model (GTM)

The model used for this research is the Simulink representation of the NASA Generic Transport Model (GTM). Importantly, its wide aerodynamic envelope allows nonlinear analysis at the high angles of attack associated with upset.

3.1 Description of the GTM

The GTM is a 5.5% dynamically scaled civil transport aircraft, which was developed for NASA's aviation safety program [7]. The physical UAV is used for the in-flight analysis of control laws and upset scenarios without the risk associated with using a full scale aircraft. The results presented here are from the Simulink model known as the 'DesignSim'. Aerodynamic data was taken from extensive wind tunnel tests of the airframe. This gives a flight envelope of $-5 \leq \alpha \leq 85^\circ$ angle of attack and $-45 \leq \beta \leq 45^\circ$ angle of sideslip [8]. The aerodynamic data is made up of static and dynamic coefficients in the form of linearly interpolated data tables. The dynamic coefficients are made up of rotary balance and forced oscillation data, blended using the hybrid Kalviste method [22]. The resulting flight mechanics model is twelfth-order, with state vector $[u, v, w, p, q, r, lat, lon, alt, \phi, \theta, \psi]$.

3.2 Implementation of the GTM

The Simulink based model was connected to AUTO within the Dynamical Systems Toolbox [32]. The linear interpolation of tabular aerodynamic data resulted in an insufficiently smooth system for numerical continuation and a number of alternative interpolation methods were investigated. Ultimately, the Simulink interpolation n-D block running cubic spline interpolation was implemented as it creates smooth data and was quicker to set up than, for example, fitting multivariate orthogonal functions [33]. No unacceptable over fitting was observed in these spline representations of the data tables.

For analysis of flight mechanics the $[u, v, w]$ body axes states used in the GTM DesignSim equations of motion are not as intuitive as the wind axes velocities $[\alpha, \beta, V]$. These states are calculated in the GTM as auxiliary variables, but, when periodic orbits are computed, the minimum and maximum values of $[\alpha, \beta, V]$ are not readily available. Therefore, in our implementation, the translational equations of motion were rewritten directly in wind axes form using expressions taken from [34].

For the bifurcation analysis presented here, the GTM is reduced to an eighth-order model. To implement this eighth-order model, the feedbacks of the unused states $[lat, lon, alt, \psi]$ were terminated and replaced by constant values (the initial conditions). This results in the reduced system with state vector $[\alpha, \beta, V, p, q, r, \phi, \theta]$. With this modification the model still captures the full dynamics of the system in body axes, except that, since altitude is fixed, the influence on the aerodynamic loads of varying air density is neglected. However, this effect is negligible in terms of the time scale associated with stability and control studies. For generating flight trajectories of the GTM in the earth axes, the full twelfth-order system is used (with lat and lon the translations relative to the position at $t = 0$). Furthermore, the actuators were neglected since their dynamics has no effect on open-loop solutions: at each of the continuation run points the control surface deflections were fixed. This reduced the complexity of the model, thus allowing a faster runtime.

4 Bifurcation analysis of the GTM aircraft

The results presented in this section are for the eighth-order open loop representation of the NASA GTM aircraft (referred to here as GTM_8ol) with state vector $[\alpha, \beta, V, p, q, r, \phi, \theta]$ and centre of gravity at the nominal location of 24% mean aerodynamic chord. The starting point of the continuation was calculated using the trim function supplied with the GTM at $\alpha = 3^\circ$ where $V = 47.34$ m/s and $alt = 243$m (800ft). This gave a GTM control parameter vector of

$$\boldsymbol{\lambda} = \begin{bmatrix} \delta_a \\ \delta_e \\ \delta_r \\ \delta_t \end{bmatrix} = \begin{bmatrix} -0.004^\circ \\ 2.58^\circ \\ 0.009^\circ \\ 22.05\% \end{bmatrix}. \tag{2}$$

The trim aileron and rudder were non-zero due to the asymmetry in the aerodynamics and the alignment effects of the engines. To initiate the study, the elevator deflection angle, δ_e, was the chosen continuation parameter, so as to emulate the pilot pulling back or pushing forward on the stick with constant throttle, while not altering the ailerons and rudder. The continuation was run in both positive and negative directions from the initial point of $\delta_e = 2.58^\circ$ and the results were computed beyond the physical elevator limits of $-30^\circ \leq \delta_e \leq 20^\circ$ to be able to detect steady state solutions that leave and re-enter the realistic parameter range.

Figure 1 shows a one-parameter bifurcation diagram in δ_e for the states α and p showing equilibrium solutions only. Figure 2 builds on this information by including the periodic solutions. In Figs. 1 and 2 the solutions lie in two distinct regions: the first at low to medium angles of attack ($\alpha \approx -5^\circ$ to 25°) and the second at higher angles of attack ($\alpha \approx 30^\circ$ to 42°). In these two regions we classify the different types of dynamics into seven regimes, labelled A—G and denoted in table 2. The regions are linked outside the physical limits of the elevator and were located by applying the continuation algorithm well beyond the realistic parameter range. The behaviour in each of these two regions is now discussed individually; subsequently in section 5 we present how these two branches are connected within the physical elevator range by using rudder deflection, δ_r, as the continuation parameter.

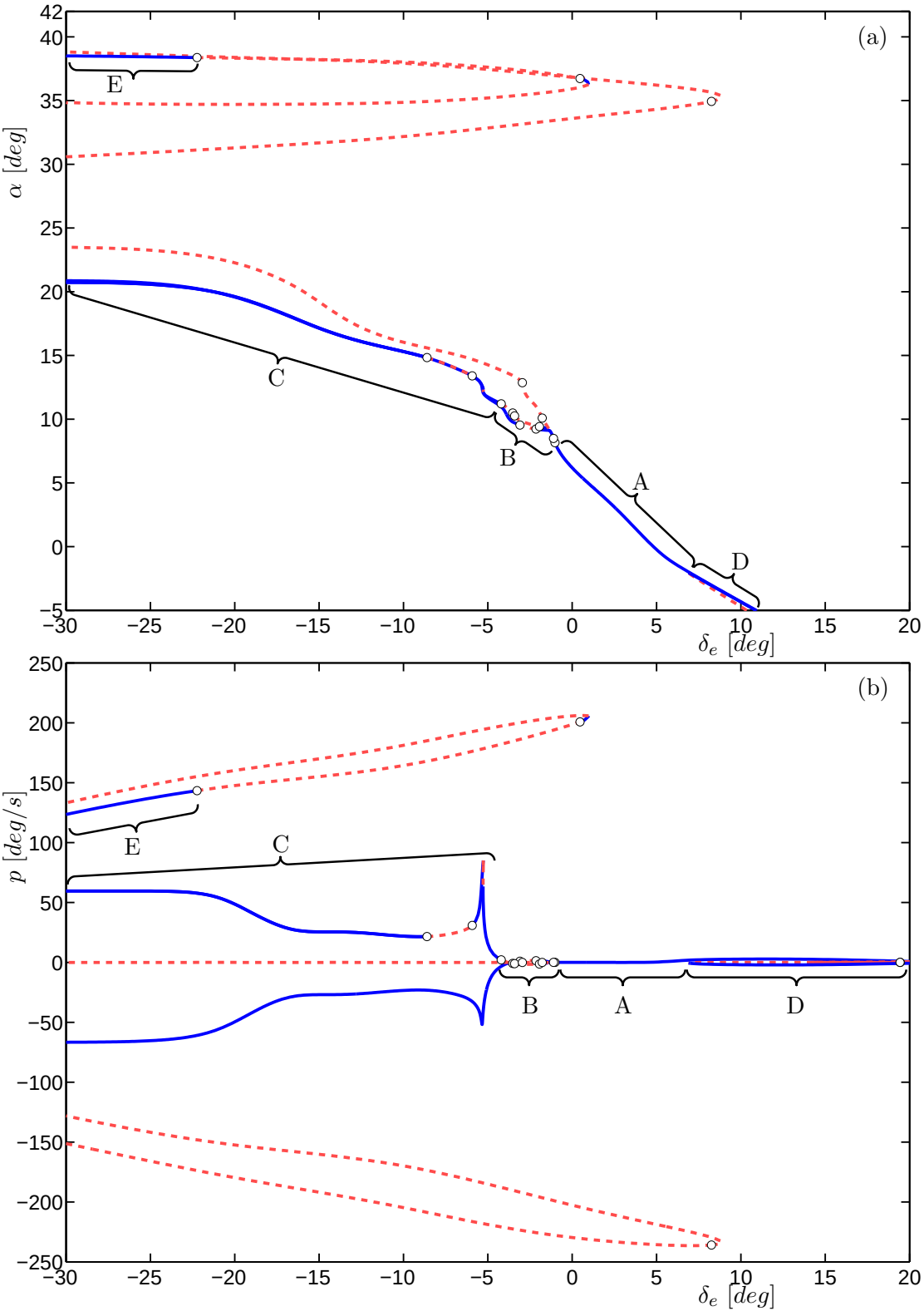

Figure 1: One-parameter bifurcation diagrams in elevator deflection, δ_e, of equilibrium solutions for GTM_8ol showing angle of attack α (a) and roll rate p (b); here $\delta_a = -0.004°$, $\delta_r = 0.009°$ and $\delta_t = 22.05\%$.

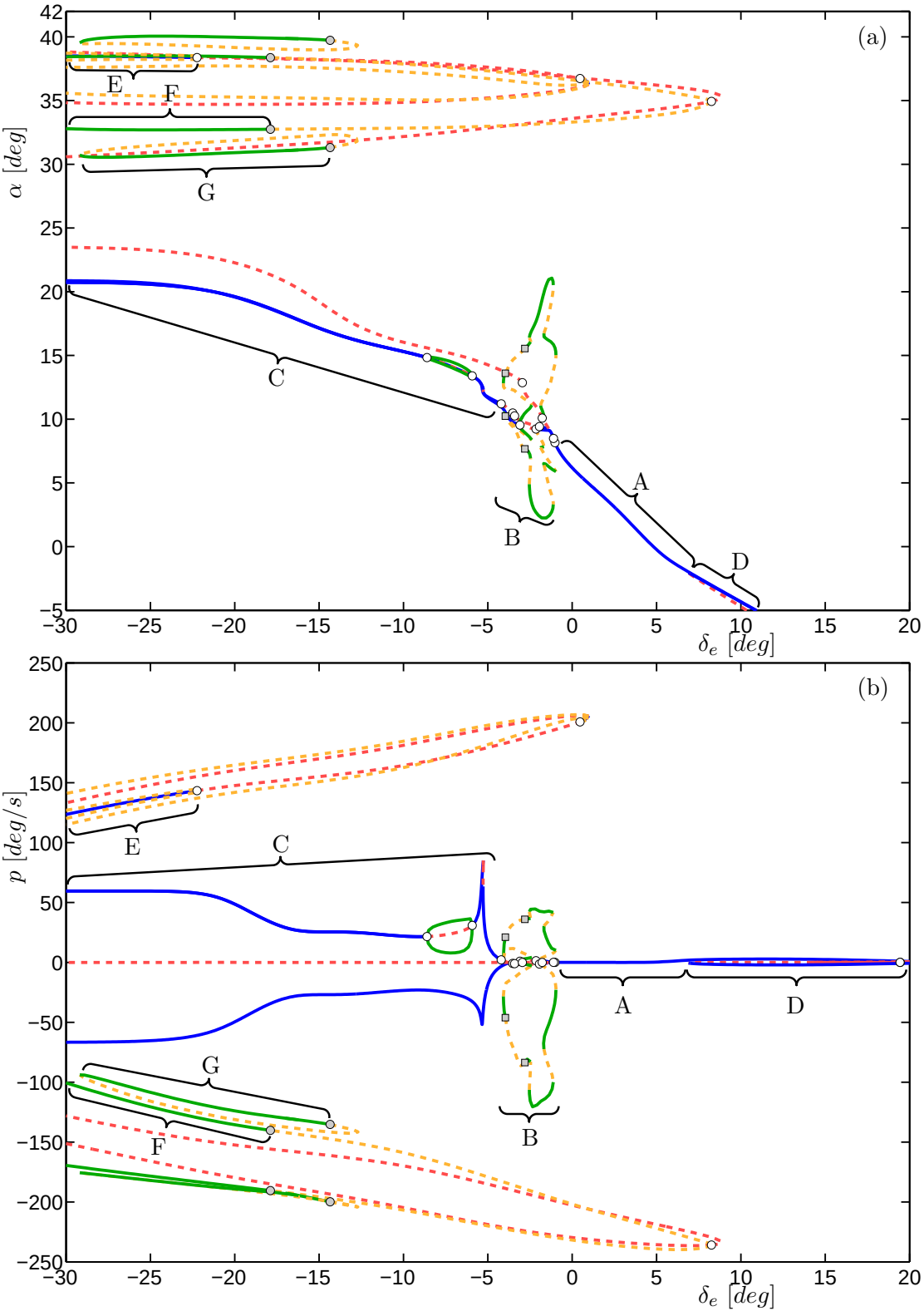

Figure 2: One-parameter bifurcation diagrams in elevator deflection, δ_e, of equilibria and periodic solutions for GTM_8ol showing angle of attack α (a) and roll rate p (b); here $\delta_a = -0.004°$, $\delta_r = 0.009°$ and $\delta_t = 22.05\%$.

Table 2: Dynamic regimes.

Symbol	Type of Dynamics	α range
A	Stable trimmed symmetric flight	$-2°$ to $8°$
B	Low frequency oscillations	$2.2°$ to $21°$
C	Steady steep spiral	$10.5°$ to $20.9°$
D	Shallow spiral	$-5°$ to $-2°$
E	Steady steep spin	$30.5°$ to $38.8°$
F	Period-one oscillatory steep spin	$32.7°$ to $38.5°$
G	Period-three oscillatory steep spin	$30.8°$ to $40°$

4.1 Low α behaviour

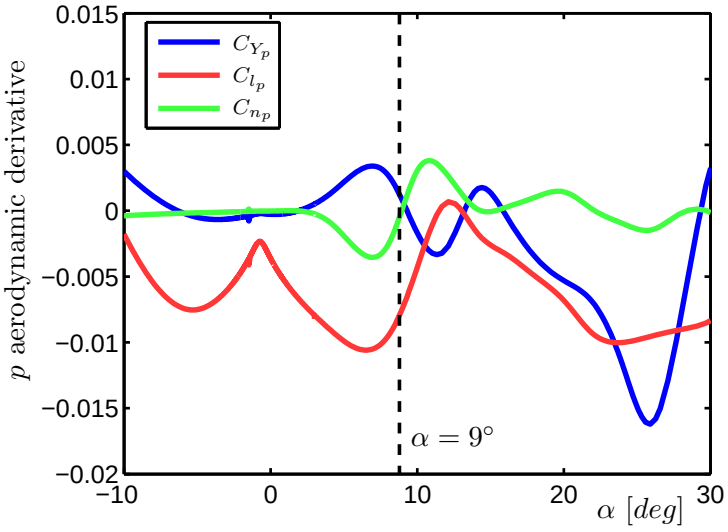

Figure 3: Aerodynamic derivatives with respect to p versus α, with the derivatives taken around the point $\beta = 0°$.

At the starting point of the continuation run ($\alpha = 3°$), GTM_8ol exhibits stable symmetric flight. As the elevator deflection decreases (i.e. the pilot pulls back on the stick), angle of attack initially increases with roll rate remaining at zero. This dynamic regime, labelled A in the α range of $-2°$ to $8°$ in Fig. 1, can be considered as the normal trimmed symmetric flight condition. As the elevator deflection decreases past $\delta_e \approx -1°$, where $\alpha \approx 8°$, GTM_8ol enters the regime of dynamics labelled B where predominantly longitudinal oscillations exist, which can be related to an unstable phugoid mode. These longitudinal oscillations arise from the Hopf bifurcations which exist in B. Within this segment, as elevator deflection decreases further through $\delta_e \approx -1.3°$ and $\alpha = 9°$ the spiral mode of GTM_8ol becomes unstable due to asymmetries in the aerodynamics. Note that this coincides with the aerodynamic derivatives C_{Y_p} and C_{n_p} changing sign; see Fig. 3. This slight spiral instability couples into the longitudinal oscillations to create the roll oscillations seen with further back stick. However, as the period of these oscillations is large ($\approx 30s$ for the subscale aircraft) and time histories have shown that these oscillations are weak attractors, the oscillations in regime B cannot be considered as upset scenarios and are, therefore, not discussed further here. More detail on this flight regime of the GTM can be found in [24].

The asymmetry grows as elevator deflection is further decreased and at $\delta_e \approx -4°$ the aircraft enters regime C where large magnitude roll departure is experienced; see Fig. 1b. Stable equilibrium branches exist to both sides of the straight and level equilibrium, although, as the aerodynamics are asymmetric, GTM_8ol is 'likely'

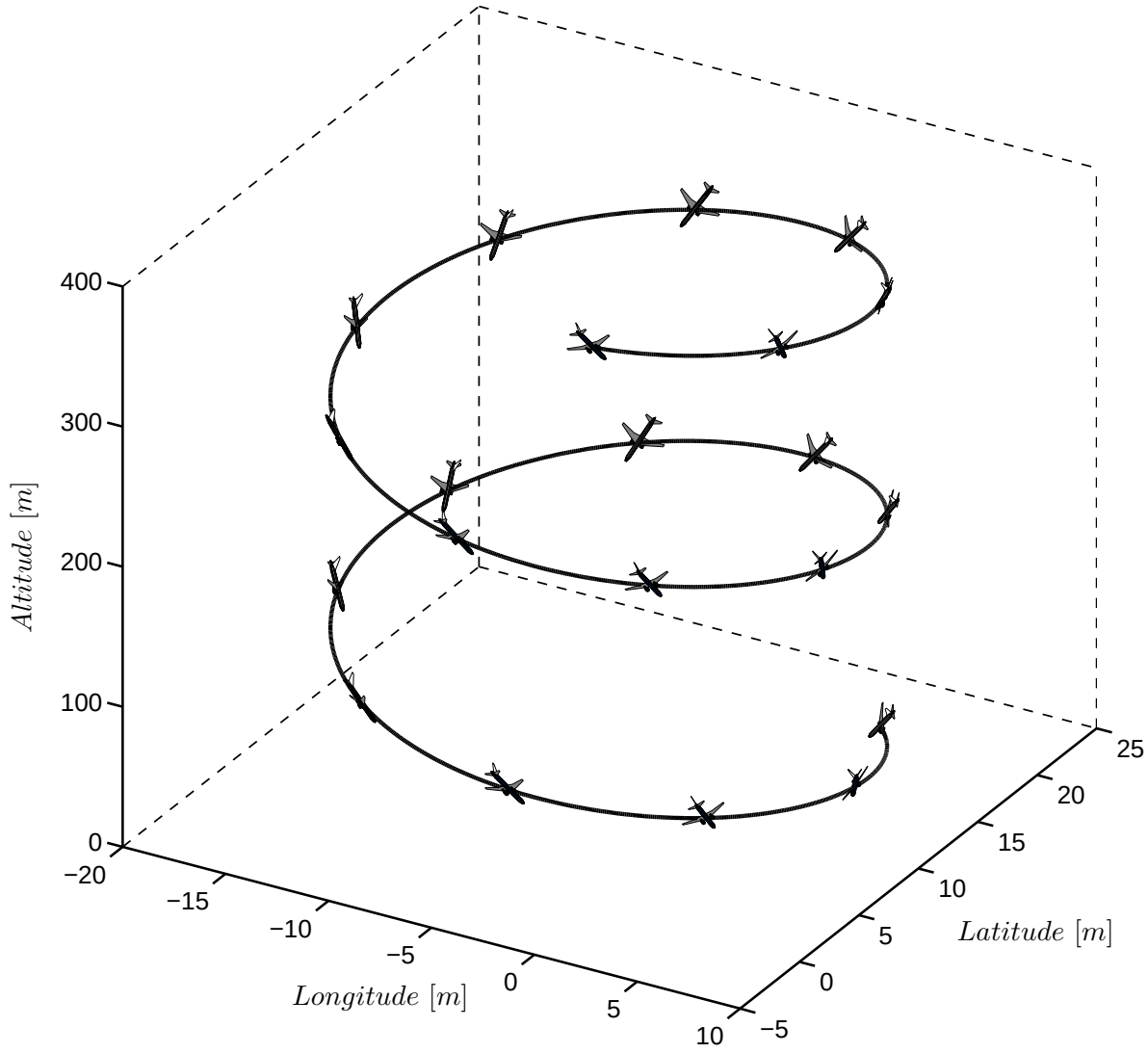

Figure 4: Trajectory of the 'steep spiral' of regime C, for $\delta_e = -30°$.

to depart to the left, i.e. with negative p. This results from the equilibrium branch representing departure to the left being connected to A through B. The equilibrium branch representing departure to the right is actually disconnected from A and reaches a limit point bifurcation where the solution folds back, becoming the unstable equilibrium where $p \approx 0°/s$. (We remark that if GTM_8ol were perfectly symmetric then it would 'prefer' neither side and any lateral instability of the zero p branch would arise at what is know as a pitchfork bifurcation [27].) Whether the aircraft spiral develops to the left or the right will in practice depend on the nature of the disturbance and/or transient dynamics. As shown in Fig. 1 these equilibrium branches of dynamic regime C do not converge on the straight and level flight branch within the physical elevator range; hence, GTM_8ol will stay on one of the two spiral branches up to and including full aft column at $\delta_e = -30°$. Regime C represents stable steady-state equilibria in the bifurcation diagram in Figs. 1 and 2. Fig. 4 is a trajectory plot from the full twelfth-order model time history; note that in this and subsequent trajectory plots, the aircraft is depicted approximately to scale with respect to latitude and longitude. The trajectory shows that regime C represents undesirable steep helical spirals. These *steep spirals* can be considered as upset conditions, although

as can be inferred from Fig. 1, GTM_8ol can be recovered easily by simply pushing forward on the stick, which matches the advice for stall recovery given in [3]. The ability to find and quantify branches like the steep spirals highlights the advantage of continuation and bifurcation analysis over linear methods, which would find the change of stability but would not easily find the stable spiral branches.

A slight lateral instability exists at low angles of attack ($\alpha \leq 0°$), labelled D in Figs. 1 and 2. This can be interpreted as a shallow spiral of GTM_8ol. However, as the lateral variables are of small magnitude (compared to C), for the purpose of this analysis, regime D is not classed as an upset condition.

4.2 High α behaviour

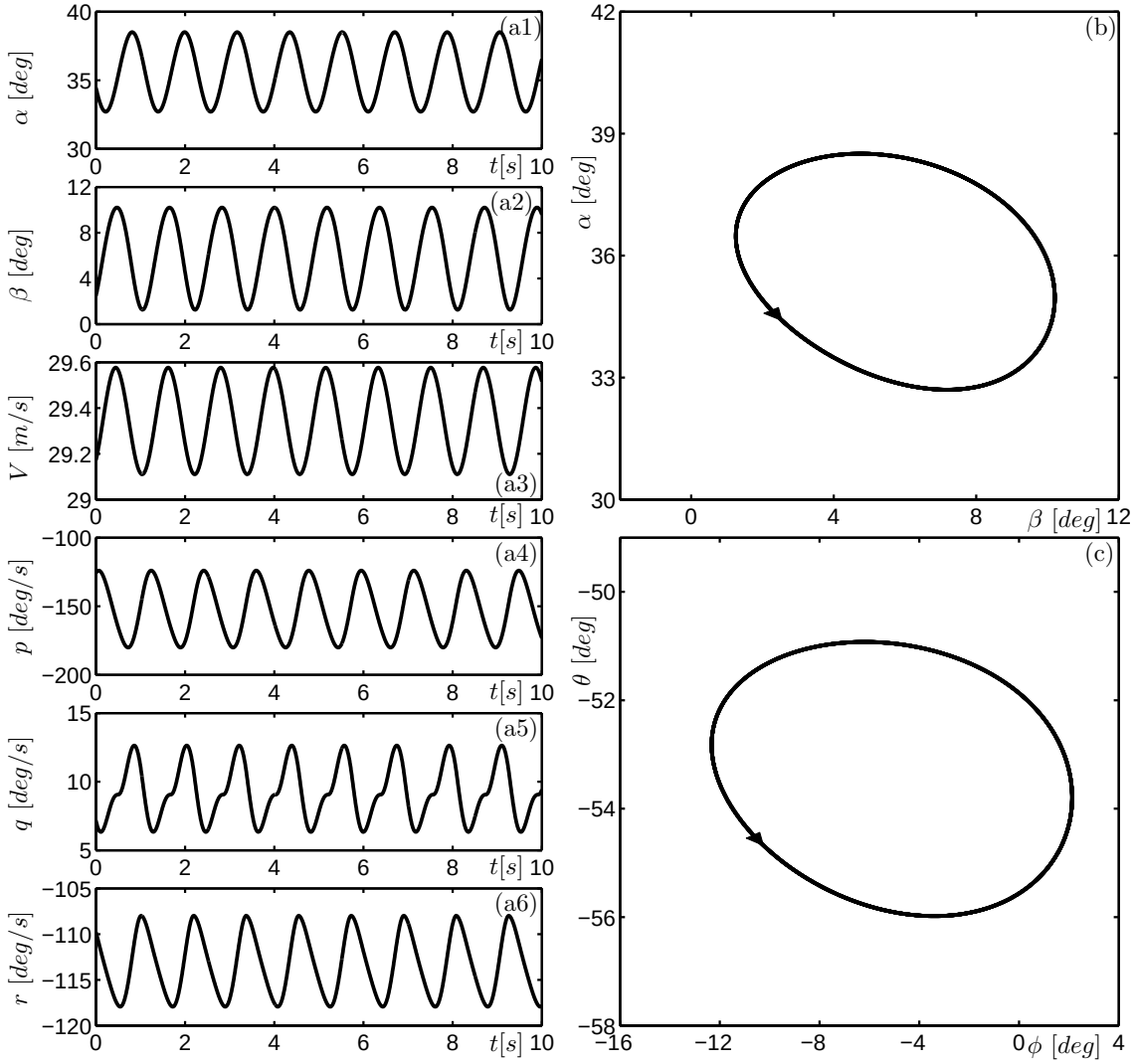

Figure 5: Time history of the period-one oscillatory spin of regime F for $\delta_e = -24°$, showing time traces of: α, β, V, p, q and r (panels a1—a6). Panels (b) and (c) show the periodic orbit in the (β,α) and (ϕ,θ)-planes, respectively.

At higher angles of attack, in the range $30° < \alpha < 40°$ in Fig. 1 and 2, additional solutions exist. First of all, there are branches of equilibria that span $-30° < \delta_e < 1°$ for positive roll rate and $-30° < \delta_e < 8°$ for negative

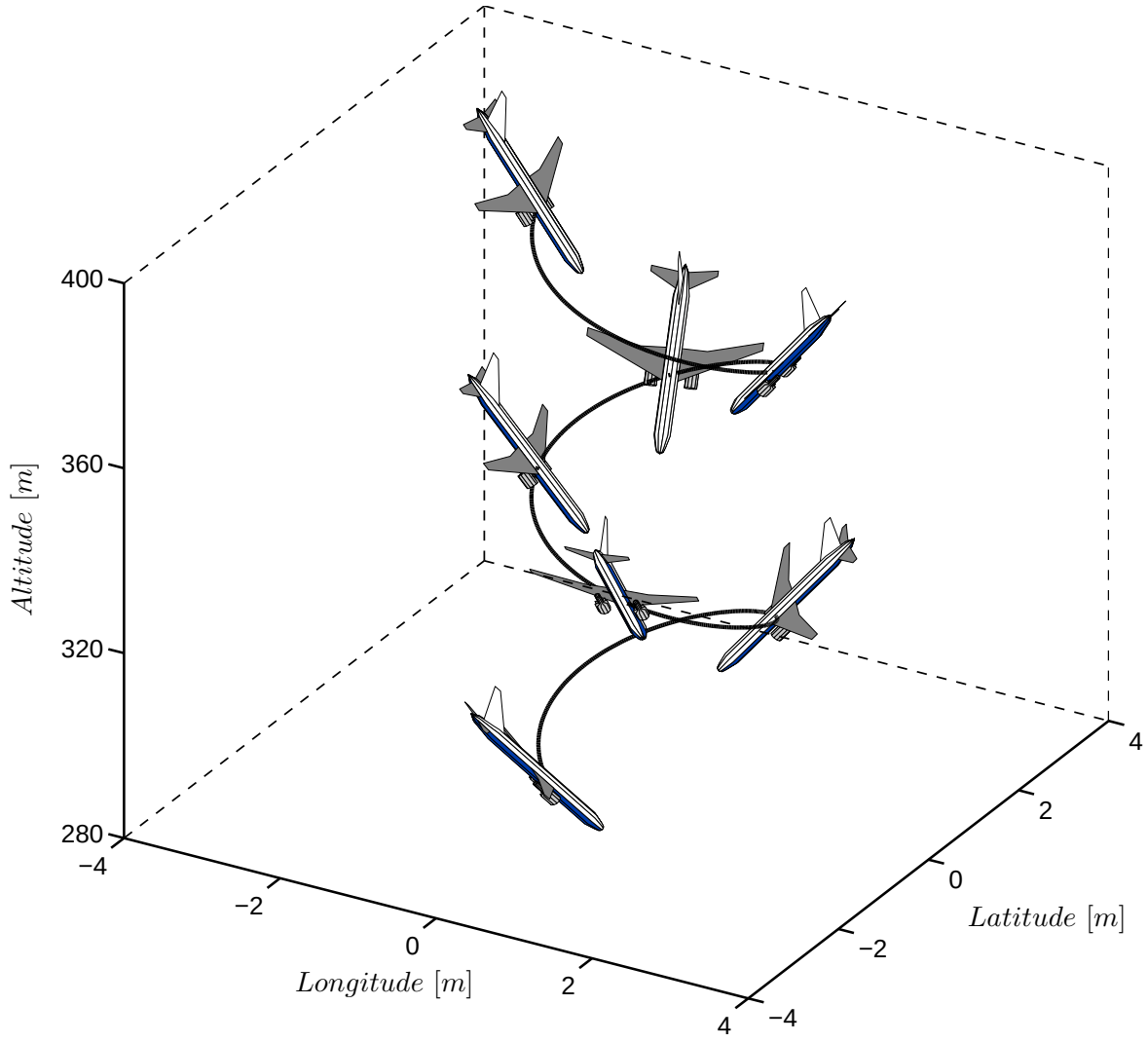

Figure 6: Trajectory of the period-one oscillatory spin of regime F for $\delta_e = -24°$.

roll rate. All these negative roll rates are unstable. However, there is a considerable region of stable equilibria with positive roll rates. These stable equilibria correspond to steady spins which we refer to as dynamic regime E. (Note that there is also a tiny region of stable spins near $\delta_e = 1°$ but this is not of practical relevance.) As regime E has a small region of attraction, this steep spin branch does not play a significant role in the upset dynamics for the chosen c.g./throttle setting. Although in the range $30° < \alpha < 40°$ the majority of equilibria are unstable and do not in themselves provide a steady spin, these solutions may influence responses in this region and this has the potential to cause chaotic behaviour. Importantly there exist three Hopf bifurcations in the valid parameter region, at $\delta_e = 0.47°$, $\delta_e = 8.26°$ and $\delta_e = -22.2°$; all occur at $\alpha > 30°$. Continuation of the periodic orbit from the Hopf bifurcations at $\delta_e = -22.2°$ and $0.47°$ show them to be unstable throughout the valid parameter range. Of more significance is the continuation of the periodic orbit from the Hopf bifurcation at $\delta_e = 8.26°$, which is initially unstable but then bifurcates to a stable periodic orbit via a torus bifurcation at $\delta_e = -17.9°$. The stable periodic orbit in regime F in Fig. 2 is of high interest as here the average angle of attack is $\alpha \approx 35°$ with high magnitude roll and yaw rates. This periodic orbit is shown in the time history and phase portrait plots for $\delta_e = 24°$ in Fig. 5. These dynamics in regime F may be regarded as an oscillatory steep spin

with a flight path angle of $\gamma \approx -89°$. The trajectory plot of this periodic orbit, in Fig. 6, shows this oscillatory spin to be much tighter than that of the steep spiral in Fig. 4. The oscillatory spins shown for the GTM in Ref. [22] also had an average angle of attack of approximately 35°: although non-zero rudder and aileron deflections were used in [22], it is typically angle of attack that dominates aerodynamic nonlinearity so that this similarity is not unexpected. Figure 2 shows that this spin mode does exist at $\delta_a \approx \delta_r \approx 0$ and $\delta_t = 22.05\%$.

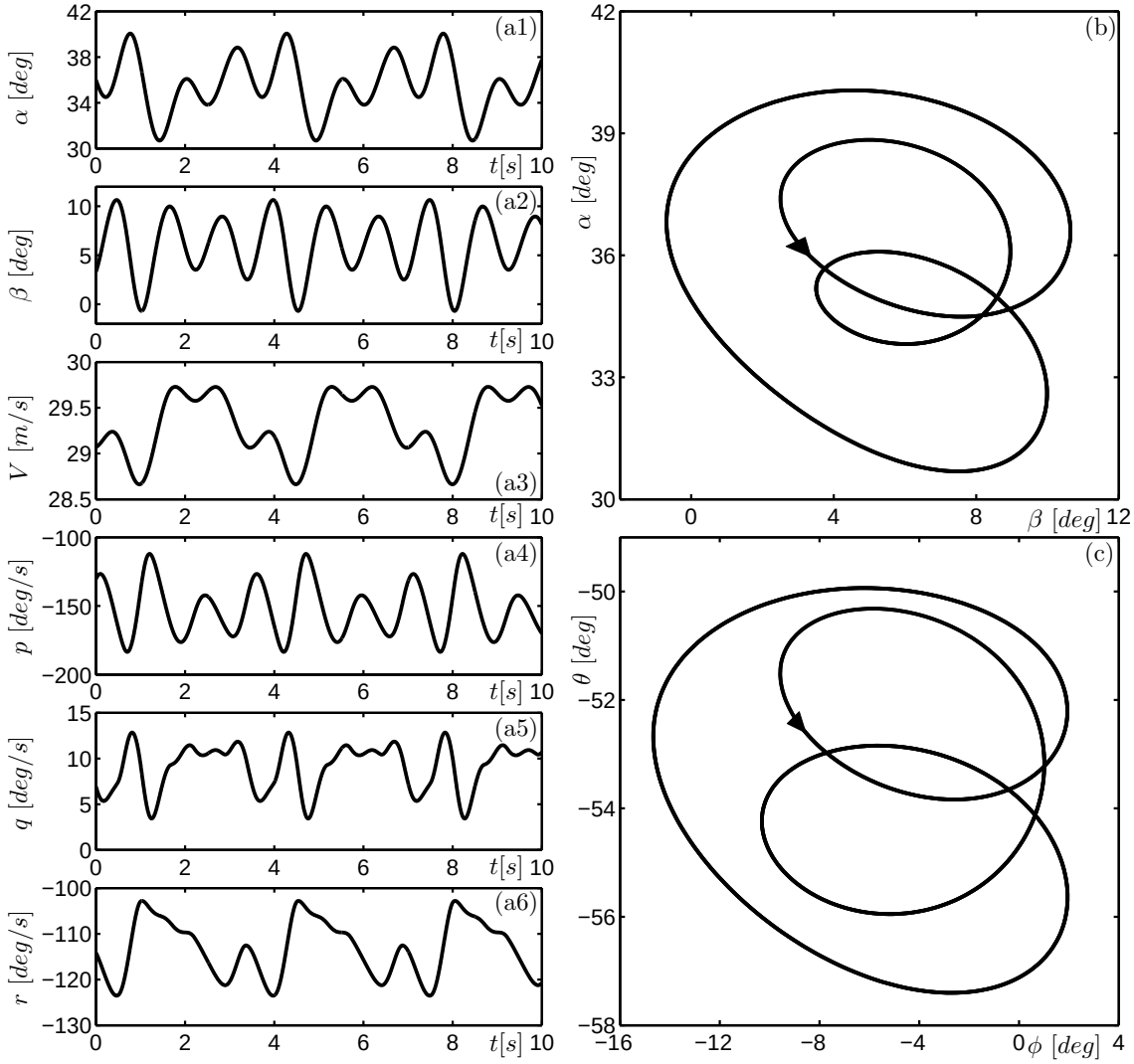

Figure 7: Time history of the period-three oscillatory spin of regime G for $\delta_e = -24°$, showing time traces of: α, β, V, p, q and r (panels a1—a6). Panels (b) and (c) show the periodic orbit in the (β,α) and (ϕ,θ)-planes, respectively.

A second stable periodic orbit was also identified in the high angle of attack region; see regime G in Fig. 2. This solution exists on an 'isola' (a closed curve that is not connected to the other bifurcation curves); it was discovered by running a time history beyond the torus bifurcation on the orbit of regime F at $\delta_e = -17.9°$. At this point this periodic orbit is no longer stable and the GTM_8ol is attracted to the periodic orbit of regime G. Figure 7 shows that regime G represents a more violent oscillation than that in regime F. Specifically, Fig. 7 shows that, it is a period-three periodic orbit, indicated by the fact that it has three amplitude maxima and minima. The trajectory plot of a time history of this period-three orbit in Fig. 8 shows that it also constitutes

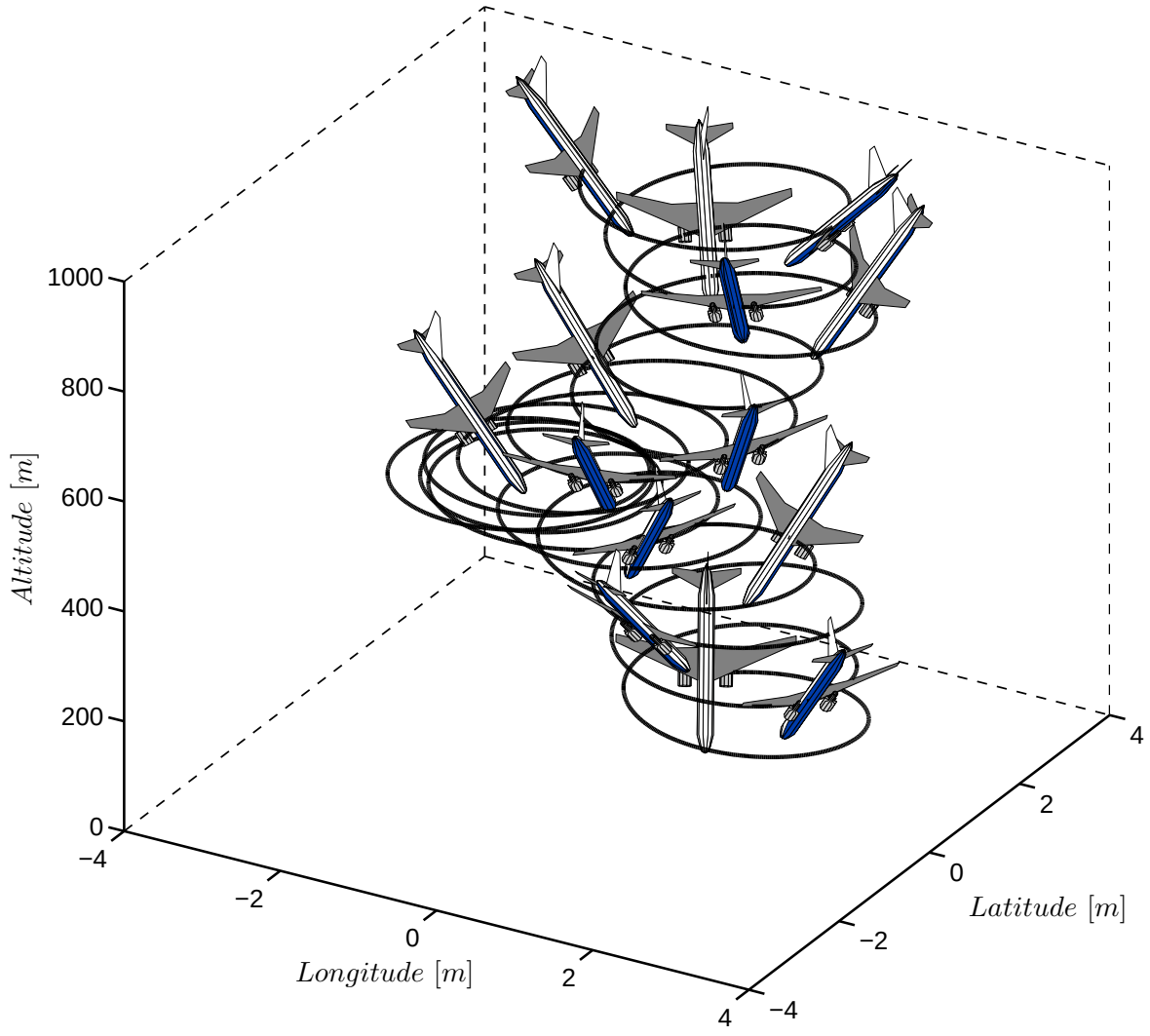

Figure 8: Trajectory of the period-three oscillatory spin of regime G for $\delta_e = -24°$.

a very tight spin mode.

The comparison of the ground-tracks of the steep spiral, the period-one periodic orbit and the period-three periodic orbit in Fig. 9 shows that there is a substantial difference in these trajectories in both scale and complexity. The steep spiral in Fig. 9a is a perfect circle, as this is a steady state solution of the eighth-order system defines in body axes coordinates; therefore, although it is spiralling, this solution has constant angular rates and angular displacement relative to the trajectory so that the radius of the spiral in the latitude-longitude plane is constant. The two periodic orbits, however, do not have constant angular rates and, therefore, the radius of the spin also oscillates. In the earth axis these appear as oscillating helixes; see Figs. 6—8. The extent of the 'wander' of the ground-track differs depending on the nature of the oscillatory solution, as the wander depends on the change of the radius during one period of the periodic orbit. The period-one periodic orbit of regime F in Fig. 9b shows little wander, and it is unlikely to be noticeable to a pilot. However, the period-three orbit of regime G in Fig. 9c exhibits a larger magnitude, easily observed wander.

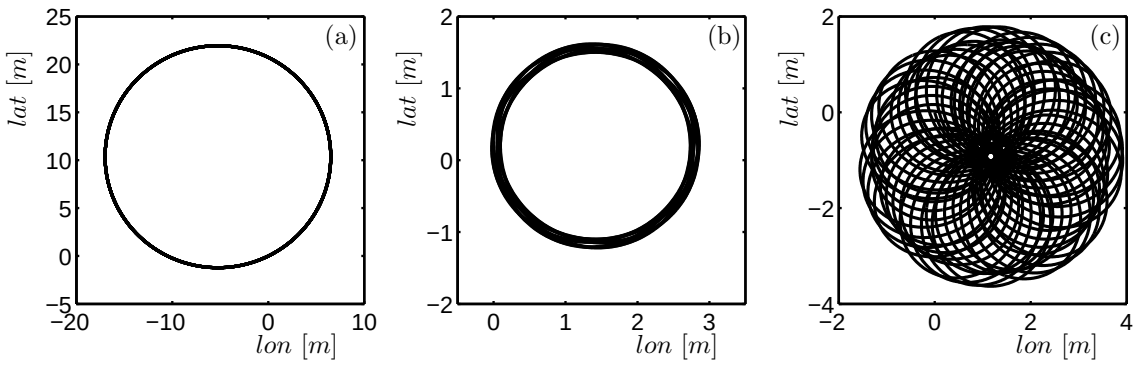

Figure 9: Ground-tracks for the steep sprial of regime C for $\delta_e = -30°$ (a), the period-one periodic orbit of regime F for $\delta_e = -24°$ (b), and the period-three periodic orbit of regime G for $\delta_e = -24°$ (c).

5 Transition from spiral to spin solutions

As mentioned in section 4, in elevator deflection alone the spiral and spin modes are only connected outside the physical elevator range, inferring that only a large external perturbation might transfer the GTM from the steep spiral to the oscillatory spins of regimes F and G. However, these solutions may still be connected within the physical δ_e range when other parameters vary. To investigate this, rudder deflection δ_r is selected as the continuation parameter and elevator deflection kept at a constant $\delta_e = -30°$, while aileron and throttle are retained at their original trim values.

Figure 10 shows the α and p projections of this one-parameter bifurcation diagram. At $\delta_r = 0.009°$, the solutions on the dotted line are the same solutions as shown at the left-hand boundary of Fig. 2 where $\delta_e = -30°$ (here c represents the solution on regime C, f_{min} and f_{max} are the minimum and maximum values of the orbit on regime F). The two stable equilibria at $\alpha \approx 21°$ are the steep spiral equilibria of regime C, and the stable periodic orbit at $32 \leq \alpha \leq 39°$ is the periodic orbit of regime F. We note that the steep spiral and oscillatory spin solutions are indeed connected within the physical rudder deflection limits for $\delta_e = -30°$. More specifically, Fig. 10 shows that, once rudder deflection is taken beyond $\delta_r \approx \pm 20°$, the GTM_8ol will enter a large oscillatory spin to either the left or right as no other stable attractors exist beyond these points. Figure 10 also shows that, once in a spin to the right (i.e. with positive lateral variables), if the rudder deflection is then returned to zero the periodic orbit becomes unstable via a torus bifurcation at $\delta_r = -4.92°$ and GTM_8ol is attracted back to the steep spiral dynamics of regime C. However, if the spin is to the left (i.e. with negative lateral variables) then, as the rudder is reduced back to zero, GTM_8ol remains attracted to the periodic orbit solutions and at $\delta_r \approx 0°$ the periodic orbit is that of dynamic regime F (for $\delta_r = 0.009$,$\delta_e = -30$) in Fig. 2 (we note that, as δ_r varies from $> 20°$ back towards $0°$, the period-one orbit does become unstable for $1° \leq \delta_r \leq 4°$; however, the resulting period-doubled orbits are stable). This confirms the earlier finding in Sec. 4.2 that the oscillatory spins only exist at zero aileron and rudder to the left with negative roll rates.

To further visualise this transition, Fig. 11 shows the results of a 50s time history which started on the steep spiral equilibrium of regime C where $\delta_r = 0.009°$, $\delta_e = -30$, $\alpha = 20.74°$, $p = 59.57°/s$, labelled point c in Fig. 10; then anti-spin (positive) rudder inputs were applied to try to counter the right steep spiral — see panel (d4) of Fig. 11. As expected from Fig. 10, once the rudder deflection exceeds $\delta_r \approx 20°$, instead of countering the steep spiral, the rudder inputs actually induce the oscillatory spin of dynamics regime F. Once in this spin, if rudder deflection is decreased back to zero then instead of returning to the spiral, the aircraft stays in the oscillatory spin to the left and tracks back down to the oscillation between F_{min} and F_{max} in Fig. 2 once $\delta_r = 0.009$. Figure 12 shows the trajectory plot of the time history shown in Fig. 11. Such a time history simulation is overlaid on top of the bifurcation diagram shown in Fig.13. This time history uses the same control surface amplitudes as in Fig. 11 but with a slower ramp input, at one tenth of the gradient, for better visualisation. Figures 11—13 demonstrates that applying rudder to get out of the spiral is an incorrect strategy for recovery from the upset

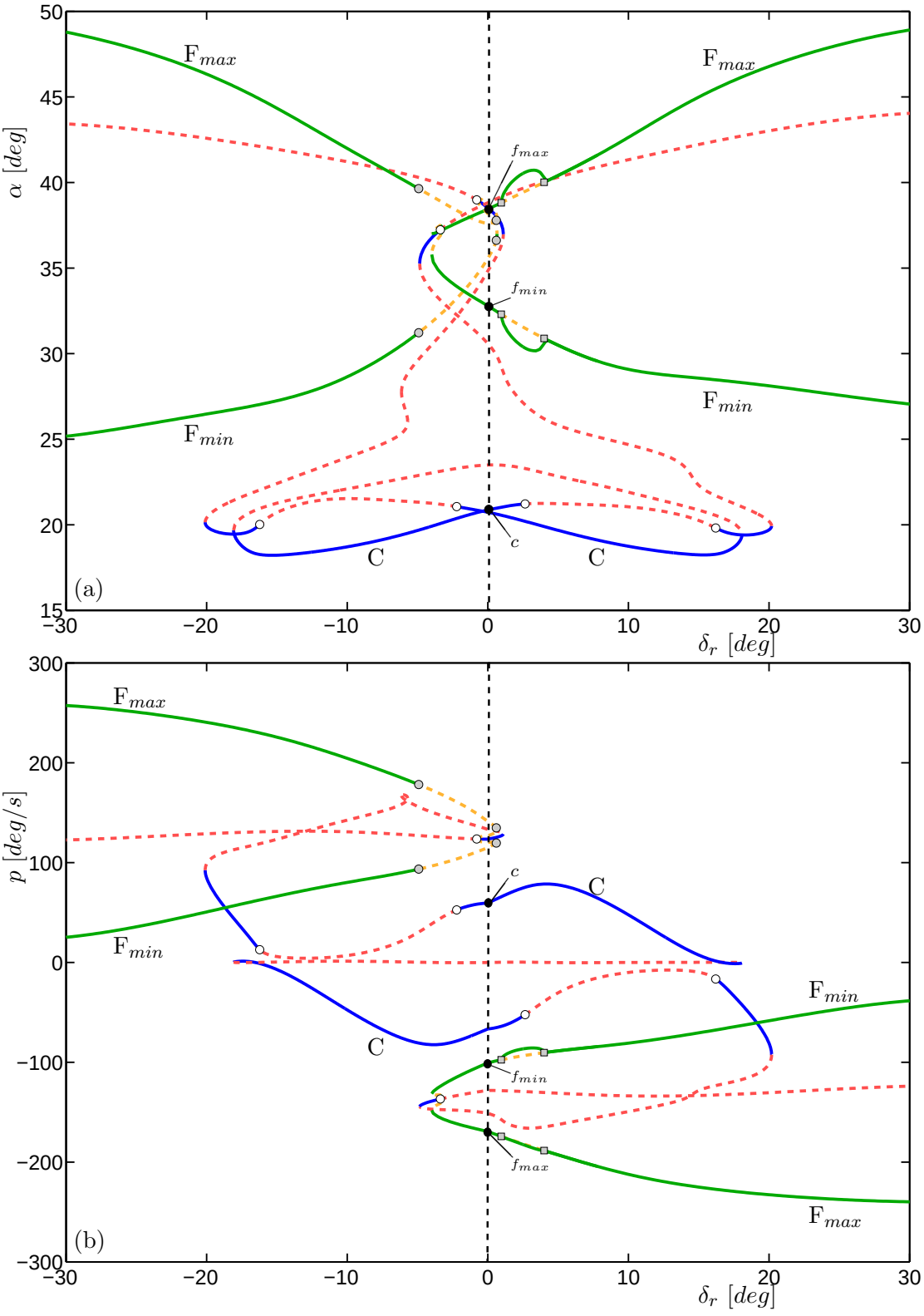

Figure 10: One-parameter bifurcation diagrams in rudder deflection, δ_r, of equilibrium and periodic solutions for GTM_8ol showing angle of attack α (a) and roll rate p (b); here $\delta_a = -0.004°$, $\delta_e = -30°$ and $\delta_t = 22.05\%$.

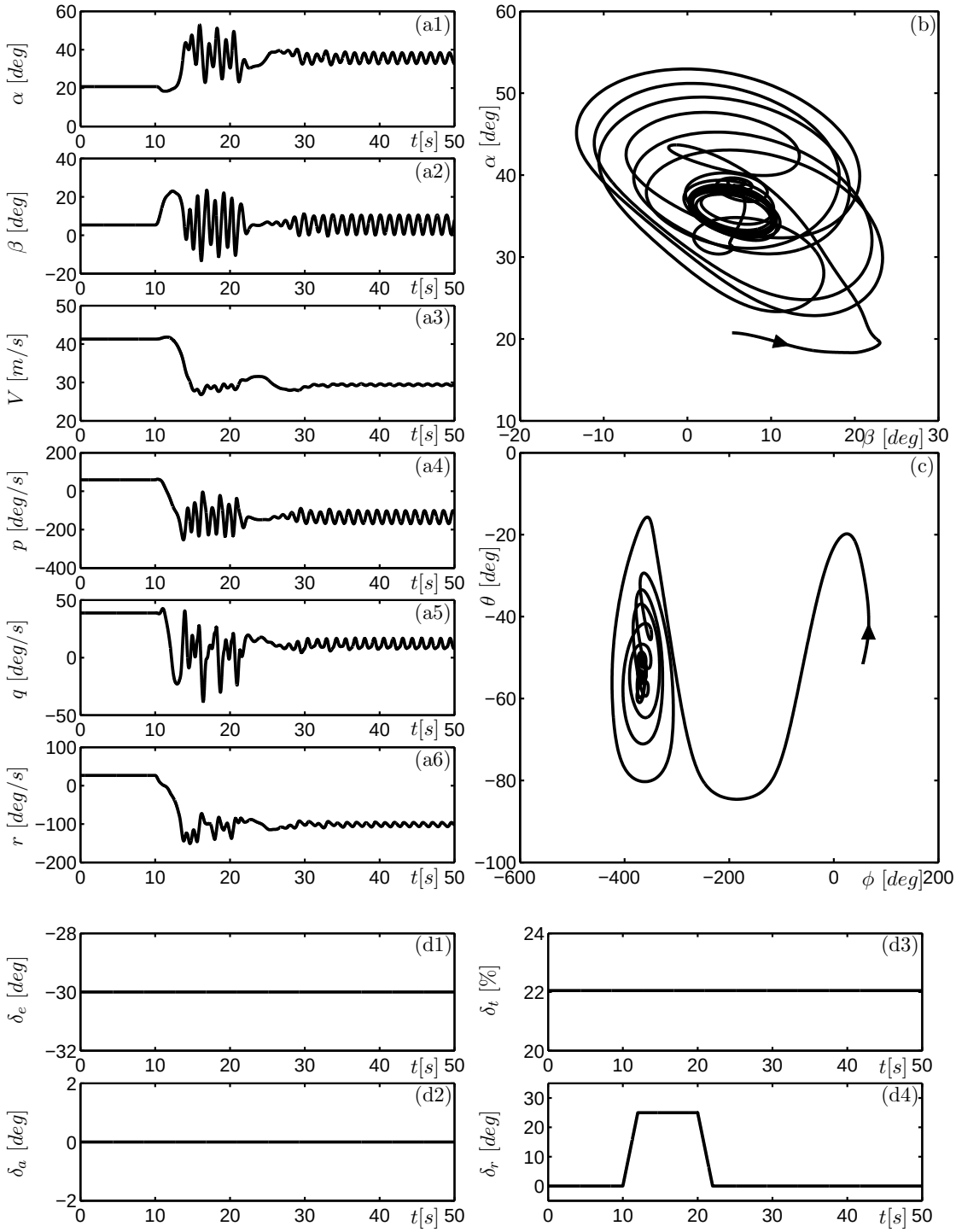

Figure 11: Time history of the mechanism for entering the period-one spin of regime F from the steep spiral or regime C, showing time traces of: α, β, V, p, q and r (panels a1—a6). Panels (b) and (c) show the corresponding trajectory in the (β,α) and (ϕ,θ)-planes, respectively; the control surface schedules are: elevator, aileron, throttle and rudder (panels d1—d4).

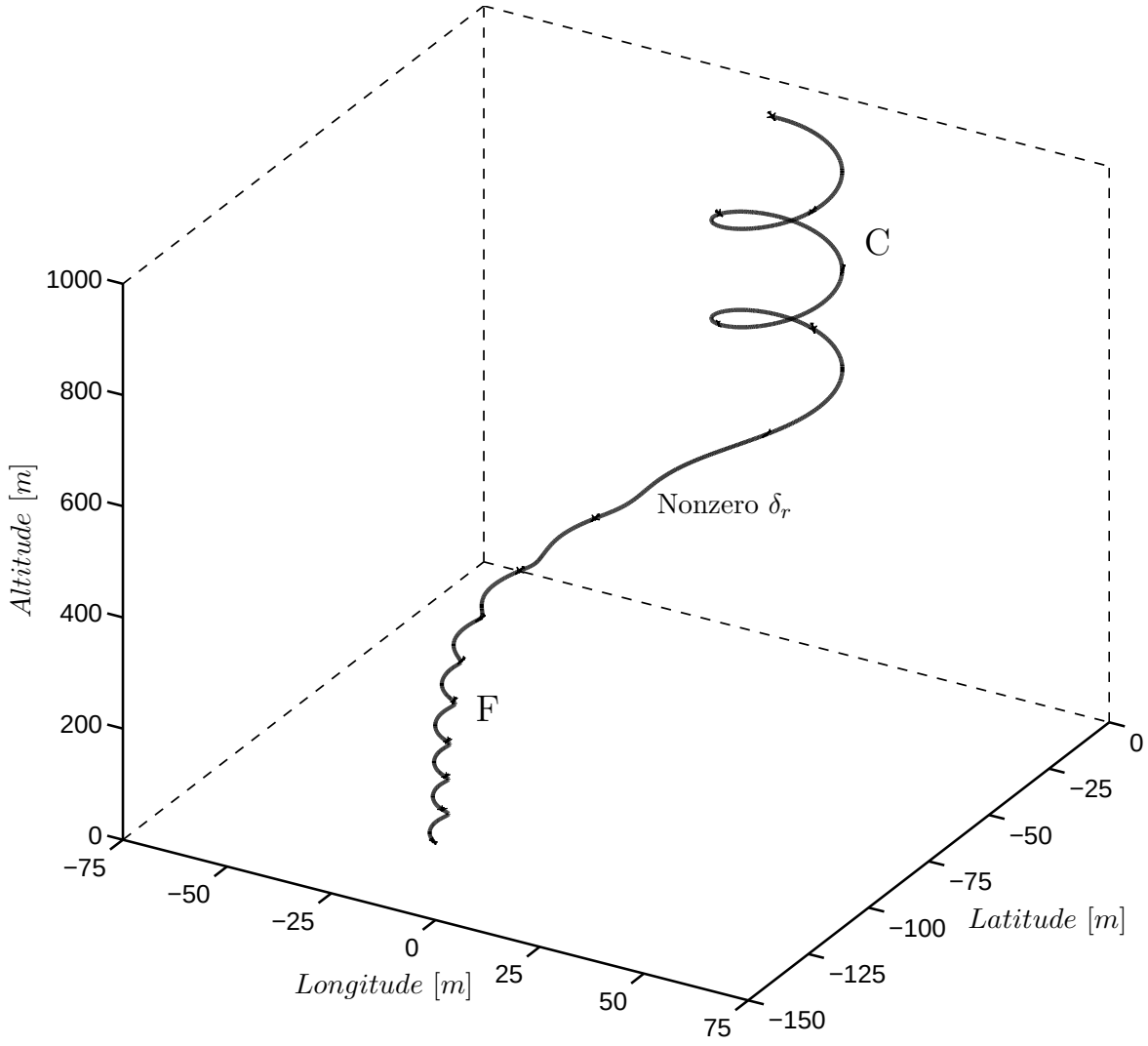

Figure 12: Trajectory of the time history from Fig. 11 showing the mechanism for entering the period-one spin of regime F from the steep spiral of regime C.

and will actually increase the severity. On the other hand, simply pushing forward on the stick, increasing δ_e to above $\delta_e = -1.3°$ and back into dynamics regime A, will recover the aircraft from both the spiral of regime C or the oscillatory spins of regime F and G (passing through regime C before reaching regime A)— given sufficient altitude.

6 Conclusion

The bifurcation analysis presented here has identified some of the rich variety of conditions governing the behaviour of the GTM; more specifically, it has found a number of stable attractors which are associated with upset. Indeed, compared to simulations that require one to wait for time history transients to disappear on weak attractors, bifurcation diagrams are much less computationally costly to create. Furthermore, bifurcation diagrams yield the underlying structure of the dynamical system and, hence, suggest where and when time histories should be run to further explain the predicted behaviour. Time history simulations have been presented

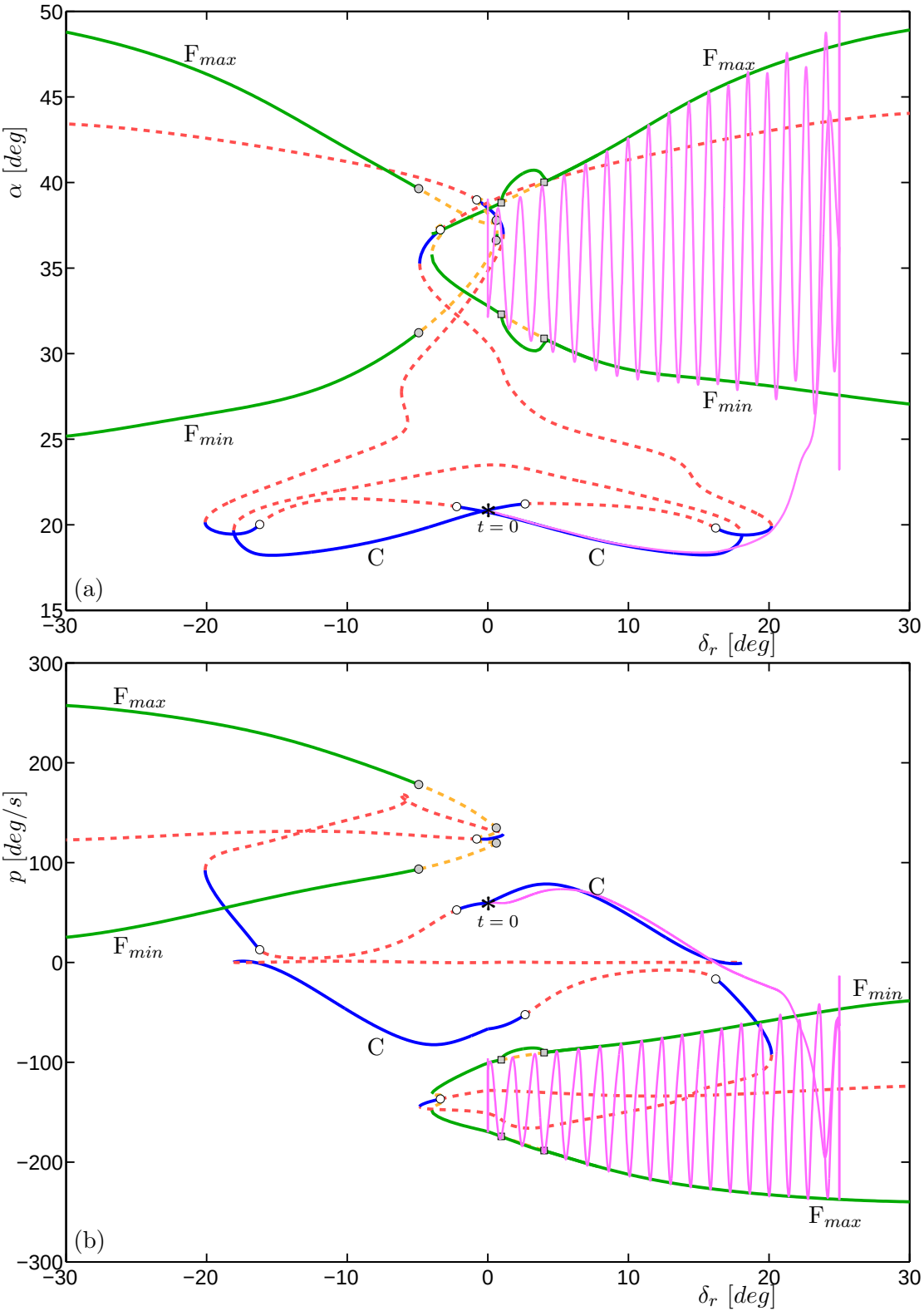

Figure 13: One-parameter bifurcation diagrams in rudder deflection, δ_r, of equilibrium and periodic solutions with a time history simulation overlaid for GTM_8ol, showing angle of attack α (a) and roll rate p (b); here $\delta_a = -0.004°$, $\delta_e = -30°$ and $\delta_t = 22.05\%$.

to complement the bifurcation diagrams to give further clarity on the nature of the different regimes of attractor dynamics. An example was presented to show how an inappropriate rudder input can lead to an oscillatory spin instead of upset recovery.

Additional open loop analysis will consider the changes to upset dynamics when parameters other than the control surface deflections are varied. An example is the centre of gravity location. Future work will also consider the upset tendencies of the GTM augmented with closed loop control systems, for example with the gain scheduled controller described in [35]. A further topic on which to focus the bifurcation analysis techniques is the upset characteristics of the GTM with the in-built 'damage scenarios' activated; these emulate some of the events described in [36]. The use of a more computationally efficient interpolation routine, such as multivariate orthogonal functions [33], could also be considered in order to improve the efficiency of future analysis. The intention is to use this information to provide an understanding of upset scenarios in civil transport aircraft and to compare the bifurcation diagrams to the upset recovery advice given in Ref. [3].

Acknowledgments

This research is supported by an Engineering and Physical Sciences Research Council (EPSRC) Award grant in collaboration with Airbus. We are grateful to members of the NASA's Langley Flight Dynamics Branch and Dynamics Systems and Control Branch for provision of the GTM model and advice on its use and flight characteristics. Discussions with Simon Pauck and Japie Engelbrecht from Stellenbosch University on implementation of the model are much appreciated.

References

References

[1] Chatrenet, D., "Air Transport Safety - Technology and Training," *ETP 2010*, May 2010, http://ec.europa.eu/invest-in-research/pdf/workshop/chatrenet%20_b3.pdf.

[2] Aviation Safety Boeing Commercial Airplanes, "Statistical Summary of Commercial Jet Airplane Accidents Worldwide Operations 1959 - 2011," Tech. rep., Boeing Commercial Airplanes, July 2012.

[3] Carbaugh, D. and Rockliff, L., "The Airplane Upset Recovery Training Aid, Revision 2," Tech. rep., The Boeing Company/Airbus, October 2008, Available from http://flightsafety.org/archives-and-resources/airplane-upset-recovery-training-aid.

[4] "Airline Safety and Federal Aviation Administration Extension Act of 2010," Public Law 111-216, Section 208, August 2010.

[5] Advani, S. and Field, J., "Upset Prevention and Recovery Training in Flight Simulators," *AIAA Modeling and Simulation Technologies Conference*, No. AIAA-2011-6698, August 2011.

[6] Fucke, L., Biryukov, V., Grigorev, M., Rogozin, V., Groen, E., Wentink, M., Field, J., Soemarwoto, B., Abramov, N., Goman, M., and Khrabrov, A., "Developing Scenarios for Research into Upset Recovery Simulation," *AIAA Modeling and Simulation Technologies Conference*, No. AIAA-2010-7794, August 2010.

[7] Jordan, T. L., Foster, J. V., Bailey, R. M., and Belcastro, C. M., "AirSTAR: A UAV Platform for Flight Dynamics and Control System Testing," *25th AIAA Aerodynamic Measurement Technology and Ground Testing Conference*, No. AIAA-2006-3307, August 2006.

[8] Foster, J. V., Cunningham, K., Fremaux, C. M., Shah, G. H., amd Robert A. Rivers, E. C. S., Wilborn, J. E., and Gato, W., "Dynamics Modeling and Simulation of Large Transport Airplanes in Upset Conditions," *AIAA Guidance, Navigation, and Control Conference and Exhibit*, No. AIAA-2005-5933, August 2005.

[9] Gregory, I. M., Cao, C., Xargay, E., Hovakimyan, N., and Zou, X., "L1 Adaptive Control Design for NASA AirSTAR Flight Test Vehicle," *AIAA Guidance, Navigation, and Control Conference*, No. AIAA-2009-5738, August 2009.

[10] Crespo, L. G., Matsutani, M., and Annaswamy, A. M., "Design of an Adaptive Controller for a Remotely Operated Air Vehicle," *Journal of Guidance, Control, and Dynamics*, Vol. 35, No. 2, March-April 2012.

[11] Belcastro, C. M. and Jacobson, S. R., "Future Integrated Systems Concept for Preventing Aircraft Loss-of-Control Accidents," *AIAA Guidance, Navigation, and Control Conference*, No. AIAA-2010-8142, August 2010.

[12] Janke, C. and Culick, F., "Application of bifurcation theory to the high-anlge-of-attack dynamics of the F-14," *Journal of Aircraft*, Vol. 31, No. 1, January 1994.

[13] Macmillen, F., "Nonlinear Flight Dynamics Analysis," *Phil. Trans. R. Soc. Lon. A*, Vol. Vol. 356, No. 1745, 1998, pp. 2167–2180.

[14] Lowenberg, M., "Bifurcation analysis of multiple-attractor flight dynamics," *Phil. Trans. R. Soc. Lon. A*, Vol. Vol. 356, No. 1745, 1998, pp. 2297–2319.

[15] Rankin, J., Coetzee, E., Krauskopf, B., and Lowenberg, M., "Bifurcation and Stability Analysis of Aircraft Turning on the Ground," *Journal of Guidance, Control, and Dynamics*, Vol. 32, No. 2, March-April 2009.

[16] Thota, P., Krauskopf, B., and Lowenberg, M., "Interactions of Torsion and Lateral Bending in Aircraft Nose Landing Gear Shimmy," *Nonlinear Dynamics*, Vol. 57, No. 3, December 2008.

[17] Knowles, J. A. C., Krauskopf, B., and Lowenberg, M. H., "Numerical Continuation Applied to Landing Gear Mechanism Analysis," *Journal of Aircraft*, Vol. 48, No. 4, July-August 2011.

[18] Kwatny, H. G., Dongmo, J.-E. T., Chang, B.-C., Bajpai, G., Yasar, M., and Belcastro, C., "Aircraft Accident Prevention: Loss-of-Control Analysis," *AIAA Guidance, Navigation, and Control Conference*, No. AIAA-2009-6256, August 2009.

[19] Dongmo, J.-E. T., "Aircraft Stall Recovery Using Nonlinear Smooth Feedback Regulators With Inputs Constraints," *AIAA Guidance, Navigation, and Control Conference*, No. AIAA-2011-6303, August 2011.

[20] Jung, D. W., *Integration of Control Allocation Methods in Bifurcation Analysis Framework*, Ph.D. thesis, University of Bristol, Bristol, UK, 2007.

[21] Kolesnikov, E. and Goman, M., "Analysis of Aircraft Nonlinear Dynamics Using Non-Gradient Based Numerical Methods and Attainable Equilibrium Sets," *AIAA Atmospheric Flight Mechanics Conference*, No. AIAA-2012-4406, August 2012.

[22] Murch, A. M. and Foster, J. V., "Recent NASA Research on Aerodynamic Modeling of Post-Stall and Spin Dynamics of Large Transport Airplanes," *45th AIAA Aerospace Sciences Meeting and Exhibit*, No. AIAA-2007-463, January 2007.

[23] Murch, A. M., *Aerodynamic Modeling of Post-Stall and Spin Dynamics of Large Transport Airplanes*, Master's thesis, Georgia Institute of Technology, Atlanta, GA, August 2007.

[24] Gill, S. J., Lowenberg, M. H., Krauskopf, B., Puyou, G., and Coetzee, E., "Bifurcation Analysis of the NASA GTM with a View to Upset Recovery," *AIAA Atmospheric Flight Mechanics Conference*, No. AIAA-2012-4648, August 2012.

[25] Pauck, S. J. and Engelbrecht, J. A. A., "Bifurcation Analysis of the Generic Transport Model with a view to Upset Recovery," *AIAA Atmospheric Flight Mechanics Conference*, No. AIAA-2012-4646, August 2012.

[26] Engelbrecht, J. A. A., Pauck, S. J., and Peddle, I. K., "Bifurcation Analysis and Simulation of Stall and Spin Recovery for Large Transport Aircraft," *AIAA Atmospheric Flight Mechanics Conference*, No. AIAA-2012-4801, August 2012.

[27] Kuznetsov, Y. A., *Elements of Applied Bifurcation Theory Third Edition*, No. ISBN #0-387-21906-6, Springer-Verlag New York, Inc., 175 Fifth Avenue, New York, NY 10010 USA, August 2004.

[28] Krauskopf, B., Osinga, H. M., and Galán-Vioque, J., *Numerical Continuation Methods for Dynamical Systems: Path following and boundary value problems*, No. ISBN #978-1-4020-6355-8, Springer-Verlag New York, Inc., 175 Fifth Avenue, New York, NY 10010 USA, July 2007.

[29] Doedel, E. J. and Oldeman Bart, E., "AUTO-07P: Continuation and Bifurcation Software for Ordinary Differential Equations," Tech. rep., Concordia University, Montreal, Canada, January 2009, Contributions by Alan R. Champneys, Fabio Dercole, Thomas Fairgrieve, Yuri Kuznetsov, Randy Paffenroth, Björn Sandstede, Xianjun Wang, Chenghai Zhang.

[30] Goman, M. G., Zagainov, G. I., and Khramtsovsky, A. V., "Application of Bifurcation Methods to Nonlinear Flight Dynamics Problems," Tech. rep., Central Aerohydrodynamic Institute (TsAGI), March 1997.

[31] Jones, C., Lowenberg, M. H., and Richardson, T. S., "Tailored Dynamic Gain-Scheduled Control," *Journal of Guidance, Control, and Dynamics*, Vol. 29, No. 6, November-December 2006.

[32] Coetzee, E., Krauskopf, B., and Lowenberg, M., "The Dynamical Systems Toolbox: Integrating AUTO into Matlab," *16th US National Congress of Theoretical and Applied Mechanics*, No. USNCTAM2010-827, US National Congress of Theoretical and Applied Mechanics, AIAA, July 2010.

[33] Morelli, E. A., "Global Nonlinear Aerodynamic Modeling Using Multivariate Orthogonal Functions," *Journal of Aircraft*, Vol. 32, No. 2, March-April 1995.

[34] Duke, E. L., Antoniewicz, R. F., and Krambeer, K. D., "Derivation and Definition of a Linear Aircraft Model," Reference Publication 1207, NASA, August 1988.

[35] Crespo, L. G., Kenny, S. P., Cox, D. E., and Murri, D. G., "Analysis of Control Strategies for Aircraft Flight Upset Recovery," *AIAA Guidance, Navigation, and Control Conference*, No. AIAA-2012-5026, August 2012.

[36] Shah, G. H., "Aerodynamic Effects and Modeling of Damage to Transport Aircraft," *AIAA Atmospheric Flight Mechanics Conference and Exhibit*, No. AIAA-2008-6203, August 2008.